Wide Range Refractive Index Measurement Based on Off-axis Tilted Fiber Bragg Gratings Fabricated using Femtosecond Laser

Xuantung Pham, Jinhai Si, Tao Chen, Fenghuang Qin, and Xun Hou

Abstract—In this paper, we propose an off-axis tilted fiber Bragg grating (OTFBG) in which the grating structure is limited to one side of the fiber core cross-section. The tilted grating planes are fabricated using a femtosecond laser with a phase mask. The wavelength range of the OTFBG cladding mode resonance could be twice that of a conventional tilted fiber Bragg grating (TFBG) with the same tilt angle. The resonance intensity of the OTFBG core mode is significantly enhanced. We also fabricate a serial-double-angle OTFBG (SOTFBG) and a parallel-double-angle OTFBG (POTFBG). The wavelength ranges of their cladding mode resonances are effectively extended. The SOTFBG and POTFBG with tilt angles of $5°$ and $10°$ possess a wavelength range of cladding mode resonances of approximately 120 nm. They are capable of measuring the surrounding refractive index (SRI) with a refractive index (RI) sensible range from 1.24 to 1.45. A significantly wide range of cladding mode resonances is achieved by a SOTFBG with tilt angles of $10°$ and $15°$, which is as wide as 215 nm. The RI sensible range of this SOTFBG is estimated to be from approximately 1.00 to 1.41, thereby making it suitable for SRI measurements in both gaseous media and aqueous solutions.

Index Terms—Fiber Bragg gratings, Fiber optics sensors, Index measurements.

I. INTRODUCTION

TILTED fiber Bragg gratings (TFBGs) have been extensively studied in the past 20 years and are considered to be important optical fiber sensor components [1-4]. The TFBG grating planes are written with a nonzero tilt angle relative to the fiber axis. This structure enables light coupling from the forward core mode to the backward propagating core and cladding modes. A core mode and series of cladding mode resonances can appear simultaneously in the TFBG transmission spectrum [1]. A TFBG with strong cladding mode resonances can be fabricated using conventional methods in which an ultraviolet (UV) laser source is used [3]. Since the UV-written gratings are dependent on the fiber intrinsic photosensitivity, the fiber is typically hydrogen loaded or increased germanium-doping level to increase its fiber core photosensitivity. Regular UV-written grating structures are easy to erase when the temperature is higher than $400°C$ [5]. To solve these problems, various TFBG fabrication methods using a femtosecond laser have recently been demonstrated [6, 7, 8]. The gratings that are formed using these methods result from the strong nonlinear interaction between the glass and a femtosecond laser. In this case, the photosensitization such as hydrogen-loading or the increasing germanium-doping level is no longer needed, and grating structures are stable at high temperatures [9, 10].

TFBG cladding modes are guided by the cladding-surrounding boundary. Since they can significantly interact with external environmental media, the TFBG is widely used in the field of surrounding refractive index (SRI) sensing [3, 11, 12]. In addition, the TFBG core mode is insensitive to the SRI but sensitive to the temperature with a sensitivity that is similar to those of cladding modes. It can be used to calibrate the temperature-induced spectral shift (which is approximately 10 pm/℃), thereby eliminating the temperature-induced cross-sensitivity in the refractive index (RI) measurement [2]. However, the core mode resonance may completely disappear when the TFBG tilt angle exceeds $6°$ [1, 7, 13]. Consequently, the TFBG with a large tilt angle could find it difficult to produce a temperature-insensitive SRI sensor using the above method. Moreover, the TFBG excited cladding modes which have their own effective indices and sensitivities to SRI changes. The RI sensible range of a TFBG is determined by the wavelength range of the excited cladding modes, which are changed according to the tilt angle. A weakly TFBG ($\leq 10°$) can be used for measuring the SRI in aqueous solutions within a specific RI range that varies from 1.30 to 1.45 [3]. A TFBG with a high tilt angle of $37°$ can allow for the excitation of cladding modes with effective indices between 0.92 and 1.18 which can be used for measuring the SRI in gaseous media [12]. Thus far, many schemes have combined several TFBGs in a device to achieve a wide range of cladding mode resonances and produce a wide-range SRI sensor [13-15]. Chen et al.

The authors are with the Key Laboratory for Physical Electronics and Devices of the Ministry of Education & Shaanxi Key Lab of Information Photonic Technique, School of Electronics & Information Engineering, Xi'an Jiaotong University, No.28, Xianning West Road, Xi'an, 710049, China (e-mail: jinhaisi@mail.xjtu.edu.cn).

X. Pham is also with Le Quy Don Technical University, Hanoi, 122314, Vietnam (e-mail: phamxuantung@stu.xjtu.edu.cn).

T. Chen is also with Xi'an Jiaotong University Suzhou Academy, Suzhou, 215125, China (email: tchen@mail.xjtu.edu.cn).

fabricated a multi-angle TFBG (MATFBG) consisting of five-concatenated TFBGs that was capable of measuring the SRI over a wide range from 1.15 to 1.45 [15]. To retain the compactness of the MATFBG (its total grating length is approximately 2 cm), its five TFBGs were carefully adjusted in their grating lengths, which were from 1 mm to 8 mm. These adjustments may increase the complexity of the MATFBG fabrication. We have recently proposed a parallel- double-angle TFBG in which two individual TFGs were inscribed in the fiber core in parallel using a femtosecond laser with a phase mask [13]. Its RI sensible range is significantly wider than that of a conventional TFBG. Furthermore, strong cladding modes have also been achieved using the particular structures of fiber Bragg gratings (FBGs) [16, 17, 18]. A type II FBG written with a femtosecond laser and a phase mask excites many cladding modes that result from the non-uniform index change across the fiber core [16, 19]. The cladding modes of the reported type II FBG are not as strong as that of the TFBG [19]. One reason for this could be that the type II FBG grating structure extends to part of the fiber cladding results in the suppression of the cladding modes [20]. D. J. Thomas et al. proposed a highly localized FBG, in which the grating modifications are inhomogeneous and asymmetric in the fiber core [17]. Such gratings enhance the coupling to the high-order cladding modes and exhibit a significantly wide range of cladding mode resonances [10, 17]. The spectral characteristic of the highly localized FBG strongly depends on the sizes and positions of the grating modifications. Until now, a highly localized FBG with a wide range of cladding modes has only been written using the point-by-point technique with a tightly focused femtosecond laser pulse, which requires a highly precise fabrication system. D. Feng et al. proposed an off-axis FBG that was inscribed only a portion of the fiber cross-section using a UV laser with a phase mask [18]. This off-axis grating structure significantly increases the coupling to the cladding modes compared with a regular FBG, thereby making it suitable for bending and physical sensing. However, up to date, there have no reports on the fabrication and spectral characteristics of a TFBG with an off-axis grating structure.

In this paper, we propose an off-axis TFBG (OTFBG) in which the grating structure is written only on one side of the fiber core cross-section using a femtosecond laser with a phase mask. The OTFBG transmission spectrum possesses a stronger core mode resonance and a wider wavelength range of cladding mode resonances compared with a conventional TFBG. The birefringence and polarization effect of the OTFBG are measured. We also fabricate a serial-double-angle OTFBG (SOTFBG) and a parallel-double-angle OTFBG (POTFBG). These double-angle OTFBGs effectively broaden the wavelength range of the cladding mode resonances and could be used to produce a wide-range SRI sensor. A significantly wide range of cladding mode resonances of 215 nm is obtained by a 10 °and 15 °SOTFBG. The RI response of the SOTFBG is investigated in aqueous solutions with an RI range from 1.33 to 1.45.

II. Experiment Methods

In our experiments, all TFBGs were written in a single-mode fiber SMF-28 (fiber core diameter ~ 8.2 μm) using a femtosecond laser with a phase mask. The schematic of the TFBG fabrication system is shown in Fig. 1 (a). A Ti: sapphire regenerative amplifier laser system (Libra-USP-HE, Coherent Inc., USA) with an operating wavelength of 800 nm and 50-fs pulse duration was adopted. The 12 mm diameter laser beam with 0.6 mJ pulse energy at 1 kHz repetition rate was focused using a cylindrical lens (focal length of 25 mm) through a phase mask (pitch of 2.142 μm) into the fiber. The fiber was positioned 3 mm away from the phase mask to generate pure interference between the ±1 st-order diffractive laser beams. The fabrication method that we previously proposed [7] was used to fabricate tilted grating planes. Using this method, the fiber scanning angle that determines the TFBG tilt angle was achieved by simultaneously scanning the fiber across its x- and y-axes. The fiber was clamped on a piezoelectric platform, which can achieve a three-dimensional translation with a maximum length of 20 μm. The scanning values of the fiber along its x- and y-axes could be set by controlling the piezoelectric platform via a computer program. Thus, the TFBGs with different tilt angles could be easily fabricated by changing the fiber scanning parameters. In the fabrication process, the focused laser beam center was precisely adjusted on the fiber core center based on the diffraction pattern of the laser beam going through the fiber. This diffraction pattern was observed on a screen that was located behind the fiber. The grating structures could be correctly written at arbitrary positions in the fiber core cross-section by setting the fiber scanning region. A broadband light source and an optical spectrum analyzer (OSA) (Yokogawa, AQ6370D) with a spectral resolution of 0.02 nm were used to monitor and record the fabricated TFBG transmission spectra.
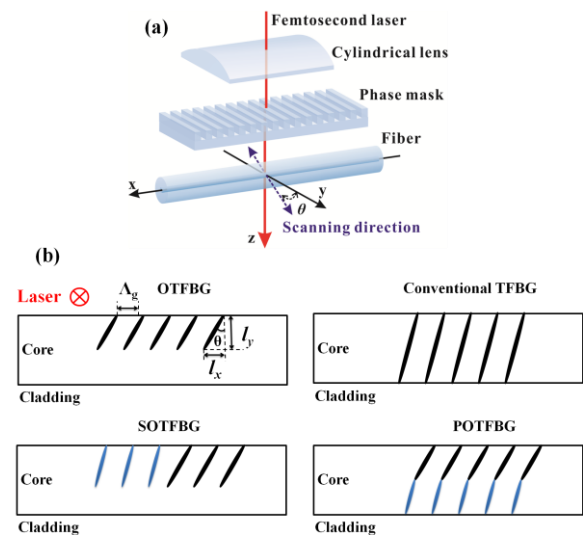

Fig. 1. (a) A schematic of the fabrication system of a TFBG using a femtosecond laser irradiation with a phase mask. (b) Configurations of the grating distributions in the fiber core of the OTFBG, conventional TFBG, SOTFBG, and POTFBG, respectively.

We fabricated four types of TFBGs including the OTFBG, conventional TFBG, SOTFBG, and POTFBG using the method

that was described above. The grating distributions of these TFBGs are shown in Fig. 1 (b). We investigated the spectral characteristic of the OTFBG and compared it with that of the conventional TFBG with the same tilt angle. The OTFBG grating structure was limited to one side of the fiber core cross-section. The conventional TFBG is a TFBG whose grating structure covers the entire fiber core [1, 7] or even extend to a part of the fiber cladding [6]. We also fabricated a SOTFBG and POTFBG, which consist of two different OTFBGs to further extend the wavelength range of the cladding mode resonances. The two OTFBGs of the SOTFBG were serially written in the fiber core. Conversely, two OTFBGs of the POTFBG were written in parallel with each other at the same position in the fiber core. Each OTFBG of the POTFBG covers precisely half of the fiber core. The spectral characteristics of the SOTFBG and POTFBG were compared with that of an STFBG, in which two conventional TFBGs were serially fabricated in the fiber core.

The tilt angle of our fabricated TFBGs was determined by scanning values of the fiber along both its x-axis (l_x) and y-axis (l_y), which could be given by $\theta = \arctan(l_x/l_y)$ [7]. The scanning value of the fiber along its y-axis (l_y) also determined the grating length in the fiber cross-section of each TFBG, as shown in Fig. 1(b). Moreover, the grating periods along the fiber axial direction of TFBGs are independent of their tilt angles and could be given by $\Lambda_g = \Lambda_m/2$, where Λ_m is the period of the phase mask [7]. As a result, the core mode resonance wavelengths of the TFBGs with different tilt angles are identical.

III. RESULTS AND DISCUSSION

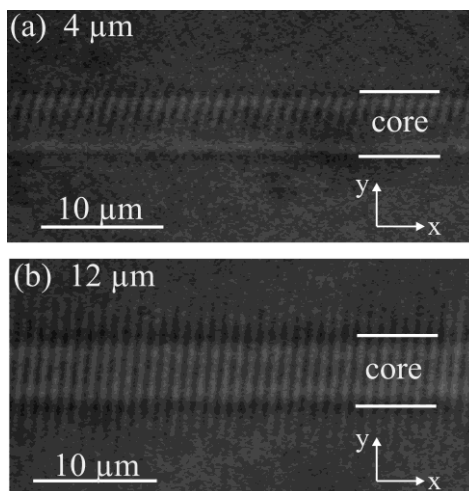#### A. Spectral characteristics of OTFBGs

Fig. 2. Optical microscope images were taken in the x-y plane of (a) an OTFBG and (b) a conventional TFBG with their transverse grating lengths of 4 μm and 12 μm, respectively.

In the fabrication process, the scanning value of the fiber along its y-axis (l_y) was set properly to obtain a TFBG with the desired grating length in the fiber cross-section. This grating length is called the transverse grating length in our discussions. The scanning value of the fiber along its x-axis (l_x) was set to the correct value to produce a TFBG with the expected tilt

angle. The microscope image in the x-y plane of an OTFBG with its transverse grating length of 4 μm is shown in Fig. 2 (a). The OTFBG grating structure correctly covers half of the fiber core. In the fabrication of conventional TFBGs, the scanning value of the fiber along its y-axis was set as 12 μm to ensure that the grating structure covers the entire fiber core and a part of the fiber cladding, as shown in Fig 2 (b). In this case, the grating structure can cover the electromagnetic field entirely, which is distributed in the fiber core and cladding (mode field diameter of approximately 10.4 μm for 1550 nm). In addition, the TFBG fabrication conditions including the laser power, laser pulse, and so on were fixed during the fabrication process. The exposure time that is required to obtain a TFBG with a saturation spectrum is directly proportional to the TFBG's transverse grating length. It varied from approximately 15 s to 60 s when the transverse grating length was from 3 μm to 12 μm. Moreover, the grating lengths and grating periods along the fiber axial direction of our TFBGs are 5 mm and 1.07 μm, respectively.
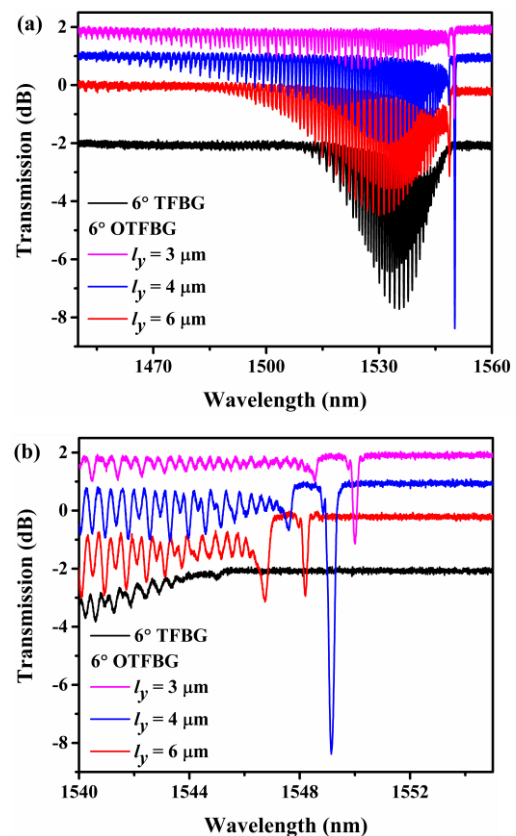

Fig. 3. (a) Transmission spectra of the 6 °conventional TFBG and 6 °OTFBGs with their transverse grating lengths (l_y) of 3 μm, 4 μm, and 6 μm, respectively. The transmission spectra are offset on the vertical axis for clarity. (b) Partially zoomed spectra of these TFBGs. The core mode resonances of these TFBGs are offset on the horizontal axis for clarity.

Table 1. Properties of those transmission spectra that are shown in Fig. 3.

Transverse grating length (l_y) (μm)	Resonance intensity of core mode (dB)	Wavelength range of cladding mode resonances (nm)	Maximum peak-to-peak intensity (dB)
3	-3.0	1450– 1548 (98 nm)	1.3

6° OTFBG	4	-9.0	1470 – 1548 (78 nm)	2.8
	6	-2.9	1490 – 1548 (58 nm)	4.1
6°TFBG	12	0	1513 – 1547 (34 nm)	5.0

We fabricated three 6° OTFBGs with transverse grating lengths of 3 μm, 4 μm, and 6 μm, respectively. The influence of the OTFBG transverse grating length on its transmission spectrum was investigated. We also fabricated a 6° conventional TFBG and compared its transmission spectrum with those of OTFBGs. The transmission spectra of the 6° OTFBGs and conventional TFBG are shown in Figs. 3 (a) and 3(b). Table 1 shows the properties of these transmission spectra including the resonance intensities of their core modes, the wavelength ranges and maximum peak-to-peak intensities of their cladding mode resonances. It can be observed that when the OTFBG transverse grating length increases from 3 μm to 6 μm, the wavelength range of its cladding mode resonances decreases from 98 nm to 58 nm. Meanwhile, the strength of its cladding mode resonances significantly increases. The maximum peak-to-peak intensity of its cladding mode resonances is enhanced from 1.3 dB to 4.1 dB. Moreover, the OTFBG transmission spectrum shows a pronounced core mode resonance. The strongest resonance intensity of its core mode reaches -9.0 dB when its transverse grating length is 4 μm, as shown in Fig. 3 (b). In contrast, the wavelength range of cladding mode resonances of the conventional TFBG is only 34 nm. Furthermore, its core mode resonance completely disappears, as shown in Fig. 3 (b). From these results, it appears that the wavelength range of the OTFBG cladding mode resonances is significantly wider than that of the conventional TFBG. The resonance intensity of the OTFBG core mode is also significantly enhanced.

To further confirm the characteristics of the OTFBG, we also investigated the transmission spectra of OTFBGs with various tilt angles and compared the results with those of the conventional TFBGs. We fabricated 4°, 8°, and 10° OTFBGs with transverse grating lengths of 6 μm. We also fabricated three conventional TFBGs with identical tilt angles. The transmission spectra of these OTFBGs and conventional TFBGs are shown in Fig. 4. Table 2 shows the properties of these transmission spectra. Compared to the conventional TFBG with the same tilt angle, the off-axis grating structure of the OTFBG significantly enhances the number of cladding modes that are excited. This enhancement is similar to the case of an off-axis FBG [18]. As a result, the wavelength range of the OTFBG cladding mode resonances could be double that of the conventional TFBG, as shown in Table 2. The wavelength range of the cladding mode resonances of the 10° conventional TFBG is only 50 nm. However, this wavelength range of the 10° OTFBG reaches up to 112 nm. Moreover, the coupling to the OTFBG core mode is also increased. The resonance of the OTFBG core mode is clearly stronger than that of the conventional TFBG. When the tilt angle of the conventional TFBG is 4°, the resonance intensity of its core mode is only -2.2 dB. When its tilt angle is 8° or 10°, its core mode resonance vanishes completely. In contrast, when the tilt angles of the

OTFBGs are 4°, 8°, and 10°, their core mode resonances are all retained with intensities of -12 dB, -3.1 dB, and -2.4 dB, respectively. The presence of the OTFBG core mode resonance is significant since it is typically used as a reference for eliminating the temperature-induced cross-sensitivity in SRI sensing [2, 11]. Due to the enhancements in the core mode resonance and the wavelength range of the cladding mode resonances, the OTFBG could be a more promising component than the conventional TFBG for producing a wide-range SRI sensor with temperature insensitivity.
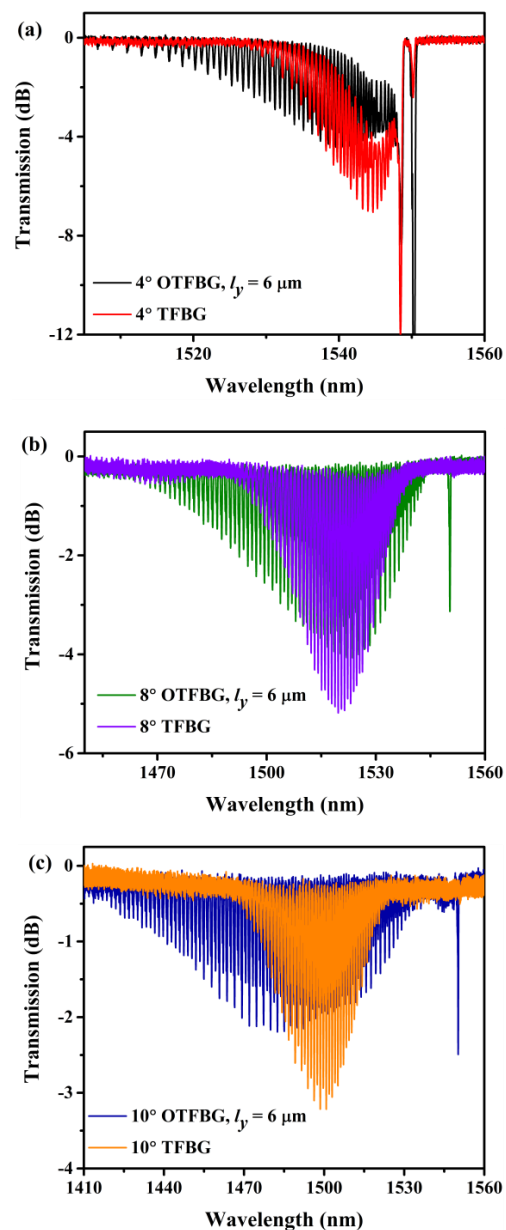

Fig. 4. Transmission spectra of (a) the 4°OTFBG and conventional TFBG, (b) the 8° OTFBG and conventional TFBG, and (c) the 10° OTFBG and conventional TFBG. The transverse grating lengths of the 4°, 8°, and 10° OTFBGs are 6 μm.

Table 2. Properties of those transmission spectra that are shown in Fig. 4.

TFBGs	Resonance intensity of core mode	Wavelength range of cladding mode resonances (nm)	Maximum peak-to-peak intensity

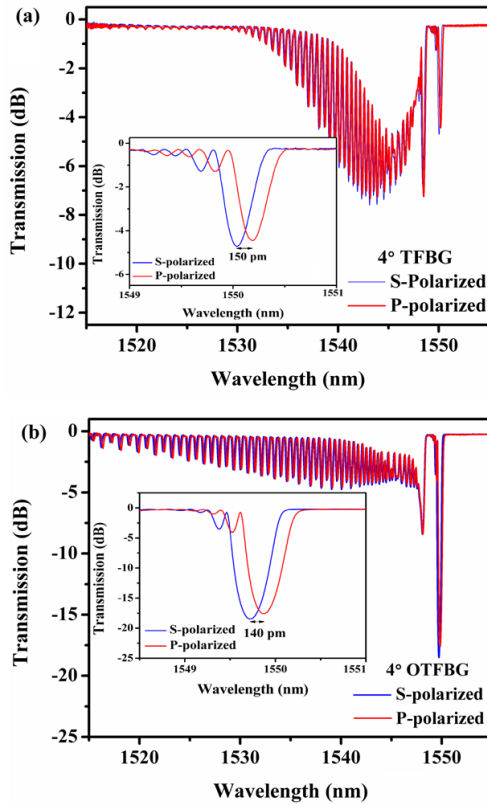|	(dB)		(dB)
4 °OTFBG	< -12	1506– 1548 (42 nm)	3.8
4 °TFBG	-2.2	1528 – 1548 (20 nm)	4.0
8 °OTFBG	-3.1	1463 – 1543 (80 nm)	3.8
8 °TFBG	0	1492 – 1539 (47 nm)	4.6
10 °OTFBG	-2.4	1420 – 1532 (112 nm)	1.9
10 °TFBG	0	1471 – 1521 (50 nm)	2.8

Fig. 5. Transmission spectra of the (a) 4 ° conventional TFBG and (b) 4 ° OTFBG when the incident core mode is polarized parallel to the tilt grating plane (P-polarized) or perpendicular to it (S-polarized). The insets show the core mode resonances of these TFBGs at two orthogonal polarization states.

We also investigated the polarization effect of our OTFBGs. Here, an in-line polarizer and a polarization controller were placed in the measurement setup between the optical source and the grating to select the orthogonal polarization states of the incident core mode. The angle of the incident polarization state was manually optimized, i.e. the incident polarization state is modified while the grating spectrum is monitored. When the incident polarization state is S- or P-polarized at the grating, different sets of cladding mode resonances become maximized [4]. Fig. 5 clearly shows that the resonance wavelengths of our TFBG core and cladding modes depend on the input polarization state. When the input polarization states are S-polarized and P-polarized, the core mode resonances are clearly separated by 150 pm and 140 pm for the 4 °conventional TFBG and 4 ° OTFBG, respectively. These wavelength separations correspond to $\Delta n \Lambda_g$ (second-order Bragg grating), where Λ_g is the grating period and Δn is the total birefringence value after the photo writing process combining the intrinsic fiber birefringence and the photoinduced one [4]. Thus, the total birefringences of the 4 ° conventional TFBG and 4 ° OTFBG are 1.40×10^{-4} and 1.31×10^{-4}, respectively. Moreover, when the incident polarization states are S-polarized and P-polarized, the wavelength separations of the core mode resonances of the 6 °, 8 °, and 10 °OTFBGs are 140 pm, 160 pm, and 170 pm, respectively. As a result, the total birefringences of these OTFBGs are calculated to be 1.31×10^{-4}, 1.50×10^{-4}, and 1.60×10^{-4}, respectively. Since the resolution of our OSA is 20 pm, the total birefringence of our TFBGs was estimated with an accuracy of about 1.87×10^{-5}. The photoinduced birefringence of our OTFBGs could be attributed to the asymmetry of the induced index profile with respect to the fiber core cross-section, which beaks the circular symmetry of the fiber core [21, 22]. The pronounced polarization effects of our OTFBGs may be applicable to single-polarization fiber laser [23]. In addition, the polarization effect of our OTFBGs should be considered to achieve high-precision measurements of the SRI or other parameters (temperature, strain, and so on).

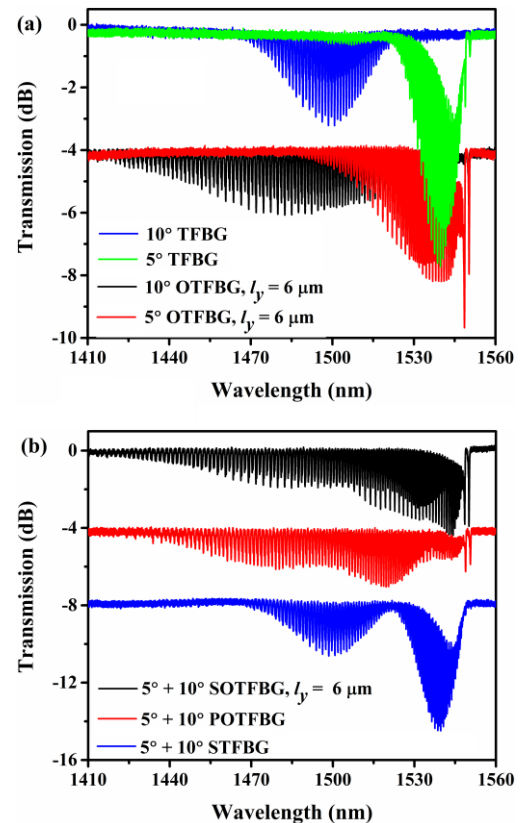B. *Spectral characteristics of double-angle OTFBGs and their application in wide-range refractive index sensing*

Fig. 6. (a) Transmission spectra of the 5 °and 10 °conventional TFBGs and the 5 ° and 10 ° OTFBGs with their transverse grating lengths of 6 µm. (b) Transmission spectra of the 5 °and 10 ° SOTFBG, POTFBG, and STFBG, respectively. The transmission spectra of these TFBGs are offset on the vertical axis for clarity.

In this experiment, we fabricated a STFBG and two double-angle OTFBGs including a POTFBG and a SOTFBG. The spectral characteristics of these double-angle OTFBGs were investigated and compared to those of the STFBG with

the same tilt angles. Since the grating length in the fiber axial direction of our fabricated TFBGs was 5 mm, the total grating lengths of the SOTFBG and STFBG were 10 mm due to their serial grating structures. Due to the parallel structure of the POTFBG, its total grating length in the fiber axial direction is still 5 mm. Consequently, the POTFBG is more compact than SOTFBG and STFBG.

To investigate the spectral characteristics of our double-angle OTFBGs and the STFBG, we firstly fabricated a 5 ° and 10 ° OTFBGs with transverse grating lengths of 6 μm. We also fabricated two conventional TFBGs with the same tilt angles. The transmission spectra of these OTFBGs and conventional TFBGs are shown in Fig. 6 (a). The spectral envelopes of the 5 ° and 10 ° conventional TFBGs are clearly separated. In contrast, the spectral envelopes of the 5 ° and 10 ° OTFBGs are partially overlapped due to the enhancement of the OTFBGs in the wavelength range of their cladding mode resonances, as previously described.

Then, we fabricated a STFBG, a SOTFBG, and a POTFBG with the same tilt angles of 5 ° and 10 °. The transverse grating length of each OTFBG in the SOTFBG was 6 μm. The transverse grating length of each OTFBG in the POTFBG was 4 μm since its grating structure covers precisely half of the fiber core. The transmission spectra of these TFBGs are shown in Fig. 6 (b). The 5 ° and 10 ° STFBG transmission spectrum is a superposition of the transmission spectra of the 5 ° and 10 ° conventional TFBGs, as shown in Figs. 6 (a) and 6 (b). The cladding modes with resonance wavelengths of approximately 1521 nm are not excited by this STFBG. Conversely, the 5 ° and 10 ° SOTFBG possesses a continuous transmission spectrum thanks to the enhancement of the wavelength range of its two OTFBGs transmission spectra, as shown in Fig. 6 (a). The wavelength range of its cladding mode resonances is approximately 128 nm (from 1420 nm to 1548 nm), which is significantly wider than that of the 5 ° and 10 ° STFBG. Moreover, its core mode resonance is preserved with an intensity of about -3.8 dB. The 5 ° and 10 ° POTFBG transmission spectrum is similar to that of the SOTFBG. The wavelength range of its cladding mode resonances is approximately 118 nm (from 1430 nm to 1548 nm). The resonance intensity of its core mode is about -2.0 dB. There is a slight difference between the envelopes of the cladding mode resonances of the SOTFBG and POTFBG, as shown in Fig. 6 (b). The reason for this could be that interactions may occur between portions of light that are coupled by both OTFBGs in the POTFBG, since they are parallel to each other. According to the wavelength range of the cladding mode resonances, the RI sensible range of the POTFBG is slightly narrower than that of the SOTFBG, but it remains of practical use for wide-range SRI sensing because of its advantageous compactness.

According to the transmission spectra of the 5 ° and 10 ° SOTFBG and POTFBG, they are suitable for measuring the SRI in aqueous solutions (RI ~ 1.30-1.45) [15]. When the cladding mode resonances of our TFBG cover a wavelength of around 1320 nm, the RI sensible range of this TFBG could be close to the air RI (~ 1.00) [12]. We fabricated an OTFBG with

a tilt angle of 15 °. The wavelength range of its cladding mode resonances covers from 1313 nm to 1455 nm (142 nm), as shown in Fig.7. We also fabricated a 10 ° and 15 ° SOTFBG, which possesses a significantly wide range of cladding mode resonances from 1313 nm to 1528 nm (215 nm), as shown in Fig. 7. Its core mode resonance is preserved with an intensity of -2.1 dB. The inset shows that all cladding modes at the shorter wavelength side of 1313 nm are suppressed in air condition (RI ~ 1.00). Based on the phase matching condition, the effective index of the cladding mode with the resonance wavelength of 1313 nm was estimated to be about 1.00, which approximately matches the air RI. Thus, the cladding mode with a resonance wavelength of 1313 nm is a cut-off mode, which is highly sensitive to the change of the air RI. In addition, the suppression of cladding mode resonances at the shorter wavelength side of 1313 nm is because these cladding modes are leaky or radiation modes, whose effective indices are lower than the air RI (the total internal reflection no longer occurs at the interface between the fiber cladding and the surrounding media) [3, 11]. These results indicate that the 10 ° and 15 ° SOTFBG, and 15 ° OTFBG could potentially be used for measuring the SRI in gaseous media [12].
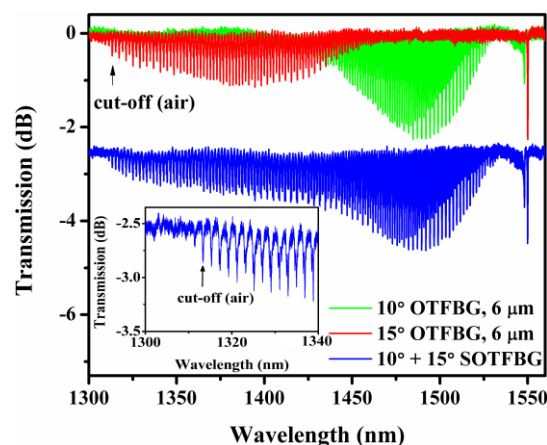

Fig. 7. Transmission spectra in air (RI ~ 1.00) of the 10 ° and 15 ° OTFBGs with transverse grating lengths of 6 μm and the 10 ° and 15 ° SOTFBG, respectively. Transmission spectra of these TFBGs are offset on the vertical axis for clarity. The inset shows a partially zoomed spectrum of the 10 ° and 15 ° SOTFBG. The arrows mark the cut-off mode positions.

Further, we investigated the RI response of our OTFBGs in aqueous solutions using the fabricated 5 ° and 10 ° SOTFBG. Aqueous glycerin solutions with various concentrations were used as the surrounding media. The refractive index of these solutions was calibrated at a wavelength of 589.3 nm using an Abbe refractometer. During this experiment, the temperature was kept at 23.5 °C. To maintain constant strain on the fiber during the experiment, the SOTFBG grating region was permanently attached to a microscope slide, and small quantities of liquids with various refractive indices were dispensed onto the grating via a pipette. Moreover, the grating region and slide were thoroughly cleaned before each measurement.

Variations of the 5 ° and 10 ° SOTFBG transmission spectra in different RI solutions with an RI range from 1.3323 to

1.4533 are shown in Fig. 8 (a). When the SRI increases, the cladding mode resonances at short wavelength side gradually disappear as these cladding modes become leaky. The cut-off mode is a boundary between the guided and leaky modes, which is usually used for SRI sensing because of its high sensitivity compared to other excited cladding modes [15]. In addition, the TFBG polarization effect significantly decreases when the cladding modes become cut-off [24]. When the SRI increases, the cut-off mode shifts monotonically towards the long wavelength side, as shown in Fig. 8 (b).
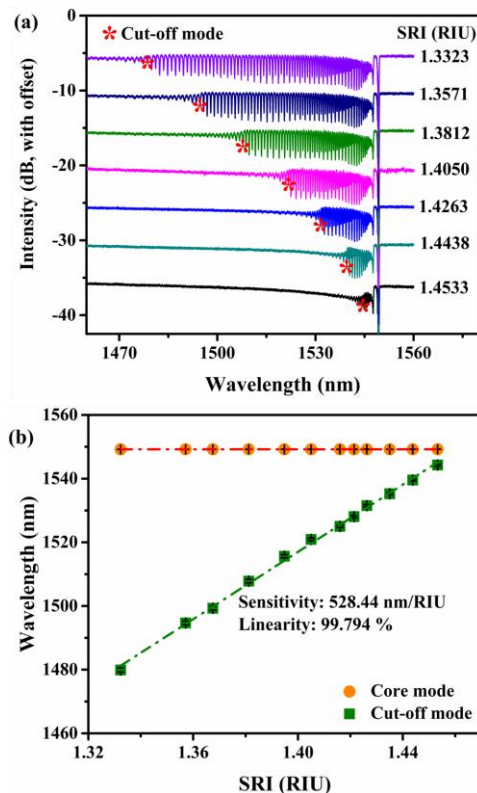

Fig. 8. (a) Variations in the 5 ° and 10 °SOTFBG transmission spectra in various RI solutions. Asterisks mark the cut-off mode. (b) The wavelength response of the cut-off and core modes of the 5 ° and 10 ° SOTFBG as a function of the refractive index of the glycerin solution at 589.3 nm. The error bars are based on the results of three measurements.

The measured cut-off wavelength as a function of the RI of glycerin solutions at 589.3 nm is shown in Fig. 8 (b). The relationship between the wavelength of the cut-off mode and the SRI is highly linear (regression coefficient = 0.99794) with a sensitivity of 528.44 nm/refractive index unit (RIU). Since the temperature was kept during our experiments, the wavelength of the core mode is constant, as shown in Fig. 8 (b). Based on the wavelength range of the cladding mode resonances and the phase matching condition, we calculated that the lower limit of the 5 ° and 10 ° SOTFBG RI sensible range could be as low as 1.22. The RI sensible range of the 5 ° and 10 ° POTFBG is similar to that of the 5 ° and 10 °SOTFBG, which is from 1.24 to 1.45. In particular, the RI sensible range of the 10 ° and 15 ° SOTFBG was estimated to be from approximately 1.00 to 1.41. Thus, the 10 ° and 15 ° SOTFBG could be used for measuring the SRIs in both gaseous media and aqueous solutions. From these results, it appears that the RI sensible range of the 10 °and

15 ° SOTFBG is wider than that of the MATFBG, which consists of five conventional TFBGs [15]. Moreover, we have previously demonstrated that the TFBG fabricated by the same method with the one that is used in this paper is stable at temperatures up to 700 ° C [7]. Thus, our OTFBGs may potentially be used for measuring the SRI at high temperatures up to 700 °C.

IV. CONCLUSION

We propose and fabricate an OTFBG using a femtosecond laser and a phase mask. The OTFBG grating structure is limited to only one side of the fiber core cross-section, which significantly enhances the coupling to the core and cladding modes. The OTFBG possesses a pronounced core mode resonance and a wide range of the cladding mode resonances, which could be double that of a conventional TFBG. The wavelength range of the cladding mode resonances is further broadened by the SOTFBG and the POTFBG. A significantly wide range of cladding mode resonances of 215 nm is obtained by the 10 ° and 15 ° SOTFBG. The RI sensible range of this SOTFBG is estimated to be from approximately 1.00 to 1.41, thereby making it suitable for measuring the SRIs in both gaseous media and aqueous media.

REFERENCES

[1] T. Erdogan and J. E. Sipe, "Tilted fiber phase gratings," *J. Opt. Soc. Am. A*, vol. 13, no. 2, pp. 296–313, Feb. 1996.
[2] C. Chan, C. Chen, A. Jafari, A. Laronche, D. J. Thomson, and J. Albert, "Optical fiber refractometer using narrowband cladding-mode resonances shifts," *Appl. Opt.*, vol. 46, no. 7, pp. 1142-1149, Mar. 2007.
[3] J. Albert, L. Y. Shao, and C. Caucheteur, "Tilted fiber Bragg grating sensors," *Laser Photonics. Rev.*, vol. 7, no. 1, pp. 83-108, Jan. 2013.
[4] C. Caucheteur, T. Guo, J. Albert, "Polarization-assisted fiber Bragg grating sensors: tutorial and review," *J. Lightwave. Technol.*, vol. 35, no. 16, pp. 3311-3322, Aug. 2017.
[5] J. Rathje, M. Kristensen, and J. E. Pedersen, "Continuous anneal method for characterizing the thermal stability of ultraviolet Bragg gratings," *J. Appl. Phys.*, vol. 88, pp. 1050–1055, July 2000.
[6] C. Chen, Y. S. Yu, R. Yang, C. Wang, J. C. Guo, Y. Xue, Q. D. Chen, and H. B. Sun, "Reflective optical fiber sensors based on tilted fiber Bragg gratings fabricated with femtosecond laser," *J. Lightwave. Technol.*, vol. 31, no. 3, pp. 455-460, Feb. 2013.
[7] R. Wang, J. Si, T. Chen, L. Yan, H. Cao, X. Pham, and X. Hou, "Fabrication of high-temperature tilted fiber Bragg gratings using a femtosecond laser," *Opt. Exp.*, vol. 25, no. 20, pp. 23684-23689, Oct. 2017.
[8] A. Ioannou, A. Thedosiou, C. Caucheteur, and K. Kalli, "Direct writing of plane-by-plane tilted fiber Bragg gratings using a femtosecond laser," *Opt. Lett*, vol. 42, no. 24, pp. 5198-5201, Dec. 2017.
[9] C. Chen, Y. S. Yu, R.Yang, L. Wang, J. C.Guo, Q.D.Chen, and H. B. Sun, "Monitoring thermal effect in femtosecond laser interaction with glass by fiber Bragg grating," *J. Lightw. Technol.*, vol. 29, no. 14, pp.2126–2130, Jul. 2011.
[10] H. Chikh-Bled, K. Chah, A. González-Vila, B. Lasri, and C. Caucheteur, "Behavior of femtosecond laser-induced eccentric fiber Bragg gratings at very high temperatures," *Opt. Lett*, vol. 41, no. 17, pp. 4048-4051, Sep. 2016.
[11] T. Guo, F. Liu, B. Guan, J. Albert, "Tilted fiber grating mechanical and biochemical sensors," *Opt. Laser. Technol.*, vol. 78, pp. 19-33, Oct. 2015.
[12] C. Caucheteur, T. Guo, F. Liu, B. Guan, and J. Albert, "Ultrasensitive plasmonic sensing in air using optical fibre spectral combs", *Nat. Commun.*, Nov. 2016. DOI: 10.1038/ncomms13371
[13] X. Pham, J. Si, T. Chen, R. Wang, L. Yan, H. Cao, and X. Hou, "Demodulation method for tilted fiber Bragg grating refractometer with high sensitivity," *J. Appl. Phys,* vol. 123, pp. 174501-174507, May. 2018.

[14] M. D. Baiad and R. Kashyap, "Concatenation of surface plasmon resonance sensors in a single optical fiber using tilted fiber Bragg gratings," *Opt. Lett.*, vol. 40, no. 1, pp. 115-118, Jan. 2015.

[15] X. Chen, J. Xu, X. Zhang, T. Guo, and BO. Guan, "Wide Range Refractive Index Measurement Using a Multi-Angle Tilted Fiber Bragg Grating," *IEEE Photonic. Tech. Lett.*, vol.29, no. 9, pp. 719-722, May. 2017.

[16] C. W. Smelser, S. J. Mihailov, and D. Grobnic, "Formation of type I-IR and type II-IR gratings with an ultrafast IR laser and a phase mask," *Opt. Express*, vol. 13, no. 14, pp. 5377-5386, Jul. 2005

[17] J. Thomas, N. Jovanovic, R. G. Becker, G. D. Marshall, M. J. Withford, A. Tunnermann, S. Nolte, and M. J. Steel, "Cladding mode coupling in highly localized fiber Bragg gratings: modal properties and transmission spectra," *Opt. Express*, vol. 19, no. 1, pp. 325-341, Dec. 2010.

[18] D. Feng, X. Gao, and J. Albert, "Off-axis ultraviolet-written fiber Bragg gratings for directional bending measurements," *Opt. Lett.*, vol. 41, no. 6, pp. 1201-1204, Mar. 2016.

[19] S. J. Mihailov, "Fiber Bragg grating sensors for harsh environments," *Sensors*, vol. 12, pp. 1898-1918, Feb. 2012. DOI: 10.3390/s120201898

[20] D. Grobnic, C. W. Smelser, S. J. Mihailov, R. B. Walker, and P. Lu, "Fiber Bragg grating with suppressed cladding modes made in SMF-28 with a femtosecond IR laser and a phase mask," *IEEE Photonic. Tech. Lett.*, vol.16, no. 8, pp. 1864-1866, Aug. 2004.

[21] Y. Lai, K. Zhou, K. Sugden, I. Bennion, "Point-by-point inscription of first-order fiber Bragg grating for C-band applications," *Opt. Express*, vol.15, no. 26, pp. 18318-18325 , Dec. 2007.

[22] P. Lu, D. Grobnic, and S. J. Mihailov, "Characterization of the birefringence in fiber Bragg gratings fabricated with an ultrafast-infrared laser," *Lightw. Technol.*, vol. 25, no. 3, pp. 779-786, Jun. 2010.

[23] Y. Lai, A. Martinez, I. Khrushchev, and I. Bennion, "Distributed Bragg reflector fiber laser fabricated by femtosecond laser inscription," *Opt. Lett*, vol. 31, no. 11, pp. 1672-1674, Jun. 2006.

[24] Y. Lu, R. Geng, C. Wang, F. Zhang, C. Liu, T. Ning, and S. Jian, "Polarization effects in tilted fiber Bragg grating refractometers", *J. Lightw. Technol.*, vol. 28, no. 11, pp. 1677-1684, Jun. 2010.